D. D. Mahoney, A. B. Mann: Nanoindentation analysis methods examined with finite element simulations

Derek D. Mahoney^a, Adrian B. Mann^{b,c}

- ^aMechanical & Aerospace Engineering Department, Rutgers University, Piscataway, USA
- ^bMaterials Science and Engineering Department, Rutgers University, Piscataway, USA
- ^cBiomedical Engineering Department, Rutgers University, Piscataway, USA

Nanoindentation analysis methods examined with finite element simulations

Quantitative mechanical properties were obtained from simulated nanoindentation load-depth curves using three analysis methods. Unloading curve fits for stiffness, depth and contact area gave reliable and relatively accurate values of elastic modulus and hardness, though inaccuracies occurred in some cases. Work of indentation analysis was effective for finding the ratio of hardness to reduced elastic modulus, but a large discrepancy occurred in one case. Fitting the loading curves with parabolas gave good fits to the simulated curves. Accurate ratios of elastic modulus to hardness were obtained for some of the loading fits, though others were inaccurate. Each method has specific strengths and weaknesses, but crucially, they all consider different aspects of the load-depth data. This means the methods are potentially complementary and a single, combined analysis may be possible and beneficial in obtaining accurate values.

Keywords: Nanoindentation; Finite element simulations; Elastic modulus; Hardness

1. Introduction

Analysis of load—depth curves to obtain accurate values of mechanical properties is an essential feature of nanoindentation testing. The ability to quantify mechanical properties directly from the load—depth data alleviates the need to image the final indentation impression, and hence, enables very shallow indents to be performed and analyzed quickly and

efficiently. Current methods of analyzing the curves are based on theoretical, continuum models for elasticity and yielding, combined with empirical fits to experimental data. Three well-known methods of analysis are based on, respectively, fits to the unloading curve, the loading curve and the area under the curves (equivalent to the work of indentation). While each of these methods has been developed over a number of years with many research groups involved they have largely become associated with specific researchers, namely: Oliver and Pharr [1] for unloading curve analysis; Hainsworth, Chandler and Page [2] for loading curve analysis; Cheng and Cheng [3] for area under the curves analysis.

There is an abundance of published papers testifying to the utility of the different methods for analyzing the curves [4-13]. Each method has its own strengths, but they also have weaknesses that are still being addressed [14-17]. Given their strengths and weaknesses it is best to view the different analysis routines as complementary rather than competing methods. The current study examined the predictive capability of these methods using finite element modeling (FEM) to obtain ideal load-depth curves for a range of materials with known elastic moduli and a variety of yield behaviors. Specifically, elastic moduli ranging from 70 GPa to 458 GPa and yield stresses that exhibit various forms of bi-linear and multi-linear isotropic hardening were used. The load-depth curves were then analyzed using the different methods. The results were compared to the FEM input values for elastic modulus, the expected hardness and the ratios of the two (i.e. either hardness to elastic modulus or hardness to reduced elastic modulus).

2. Analysis methods

2.1. Unloading curve analysis

A number of researchers have worked on methods for analyzing the unloading portion of a load-depth curve including Loubet et al. [18, 19] and Doerner & Nix [20]. Their work, along with that of earlier Russian researchers [21], was developed into what has become the "standard method" of analysis for nanoindentation testing by Oliver & Pharr [1]. It has subsequently been refined several times by way of small modifications that increase its accuracy [22]. The basis of the analysis is fitting the initial slope of the unloading curve to obtain the contact stiffness (S) that can be related to the reduced elastic modulus (E_r) of the test sample. The material's hardness is determined in the conventional manner from the peak load divided by the projected contact area (A_c) of the indentation impression. This area is obtained from the contact depth, which is also found from fitting the unloading curve.

The basis of the unloading curve technique is in part derived from earlier work done by Sneddon [23, 24], who considered the analysis of the elastic contact between a rigid, axisymmetric punch and an elastic half space. This revealed the general relationship between load on the punch and its depth of penetration. Applying this to the analysis of the unloading curve, it has been found to fit an equation of the form:

$$P = \beta (h - h_{\rm f})^m \tag{1}$$

In the above equation, P represents the indenter force or load, h is the depth of the indenter with $h_{\rm f}$ being the final (unloaded) depth of the indentation. The parameters m and β are determined from a curve fitting process. This relationship is essentially the same as that predicted by Sneddon [23, 24] when considering purely elastic deformation with the elastic depth being $h-h_{\rm f}$. This type of fit assumes that in most cases the unloading curve can be treated as purely elastic. A linear unloading curve, equivalent to m=1, is expected when a flat punch is used on an elastic half-space. This was the fit used by Loubet et al. [18, 19], and Doerner & Nix [20] to analyze nanoindentation data. The analysis of Oliver & Pharr [1] recognized that m is usually larger than 1, and m=1.5 (equivalent to a paraboloid punch) is a better approximation than a flat punch.

The standard definition of contact stiffness, *S*, is the derivative of the unloading curve. An established relationship between this stiffness and the material's reduced elastic modulus is known [25] and given by Eq. (2). In the unloading analysis elastic modulus is found from the contact stiffness for the initial part of the unloading curve by applying Eq. (2):

$$S = \frac{2}{\sqrt{\pi}} E_{\rm r} \sqrt{A_{\rm c}} \tag{2}$$

where A_c is the projected contact area, which is also used to find hardness (H) from the peak load (P_{max}) using:

$$H = \frac{P_{\text{max}}}{A_{\text{c}}} \tag{3}$$

The reduced elastic modulus, $E_{\rm r}$, is related to the indenter tip and substrate elastic properties, where $E_{\rm t}$, $v_{\rm t}$, $E_{\rm s}$, $v_{\rm s}$ are

the elastic modulus and Poisson's ratio of the tip and sample, respectively, by:

$$\frac{1}{E_{\rm r}} = \frac{\left(1 - v_{\rm t}^2\right)}{E_{\rm t}} + \frac{\left(1 - v_{\rm s}^2\right)}{E_{\rm s}} \tag{4}$$

The elastic modulus, E_t , and Poisson's ratio, v_t , of a diamond indenter tip are 1 141 GPa and 0.07, respectively.

The importance of fitting the unloading curve accurately and determining the contact area, $A_{\rm c}$, to obtain values for $E_{\rm r}$ and H is central to the analysis. To find the value of $A_{\rm c}$ a function relating it to the contact depth, $h_{\rm c}$, is needed. For a perfect Berkovich pyramidal indenter tip this would be $A = 24.5 \ h_{\rm c}^2$, but since making a perfect tip is impossible, an expanded equation is used:

$$A(h_{c}) = 24.5 h_{c}^{2} + \sum_{i=1}^{7} C_{j} \sqrt[2^{i}]{h_{c}}$$
 (5)

where C_j are calibration constants of the specific indenter tip being used. These values are obtained by performing nanoindents to a range of depths on a test material with known properties, usually fused silica. Finding the contact depth is tricky, but using largely empirical fits, it has been found that:

$$h_{\rm c} = h_{\rm m} - h_{\rm s} \tag{6}$$

where $h_{\rm m}$ is the maximum indenter depth at peak load and $h_{\rm s}$ is given by:

$$h_{\rm s} = \varepsilon \frac{P}{S} \tag{7}$$

The constant ε is taken to be 0.75 for a paraboloid contact, but ranges between 0.72 (conic indenter) and 1 (flat-punch).

The unloading analysis has been used with finite element methods in the past to help determine the mechanical properties of materials (see for instance the work of Knapp et al. [26]. FEM of indents has also been an essential part of refining the unloading curve analysis. Several significant developments [22] have been made to the standard analysis routines that address issues typically due to errors in the calculated contact depth or contact area of the indentations [27–30]. FEM methods have been instrumental in understanding and overcoming many of these limitations of the unloading curve analysis [14, 27, 29–32]. However, the basic approach of (1) fitting to the unloading curve, (2) finding the contact stiffness, (3) finding the contact area, and then (4) calculating mechanical properties from these has remained essentially the same.

2.2. Loading curve analysis

Hainsworth et al. [2, 33] took a fundamentally different approach to analyze nanoindentation data based on fitting the loading curve rather than the unloading curve. They studied a variety of materials and found that during loading, the load is proportional to the square of the indentation depth, so that:

$$P = K_{\rm m}h^2 \tag{8}$$

Int. J. Mater. Res. (formerly Z. Metallkd.) 110 (2019) 2

where $K_{\rm m}$ is a proportionality term that depends on the material's properties. From basic considerations of the elastic and plastic properties of a material they developed the following expression for $K_{\rm m}$ in terms of E and H:

$$K_{\rm m} = E \left(\varphi \sqrt{\frac{E}{H}} + \psi \sqrt{\frac{H}{E}} \right)^{-2} \tag{9}$$

The two parameters Φ and ψ have values that must be optimized for the specific indenter tip being used as all tips have slightly different geometries. This is achieved with a regression analysis of data from a number, n, of different materials (labelled "i") with known hardness, H_i , and elastic modulus, E_i . The value of K_i for each material is found from fitting to the loading curves. To find the optimum values of Φ and ψ , it is necessary to find the unconstrained minimum of the expression shown below such that the square of the errors are minimized. That is:

$$\min \sum_{i=1}^{n} \left(\varphi \sqrt{\frac{E_i}{H_i}} + \psi \sqrt{\frac{H_i}{E_i}} - \left[\frac{K_i}{E_i} \right]^{-1/2} \right)^2 \tag{10}$$

Once Φ and ψ are determined Eqs. (8) and (9) can be used to find the ratio of E to H, or if one of them is already known then the other can be found.

2.3. Work of indentation analysis

A fundamentally different method of analysis considers the work of indentation and has the advantage that it avoids the need to fit either the loading or unloading curves. Instead, the method looks at the area under the load–depth curves which can be found directly from the load–depth data. This method, as put forward by Cheng & Cheng [3, 34], facilitates the quantification of a material's mechanical properties by asserting that the area under the loading curve equals the total sum of the elastic and plastic work of indentation, while the area under the unloading curve is only the elastic work of indentation. The difference between the areas under the curves is then the irreversible (or plastic) work of indentation. The work analysis establishes an approximate relationship between the ratio of hardness to reduced elastic modulus (H/E_T) and

the ratio of irreversible work to total work. The relationship has the form:

$$\frac{H}{E_{\rm r}} \approx \Pi_{\theta} \left(1 - \frac{W_{\rm u}}{W_{\rm tot}} \right) \tag{11}$$

where $W_{\rm u}$ is the area under the unloading curve and $W_{\rm tot}$ is the area under the loading curve. Combining this with an

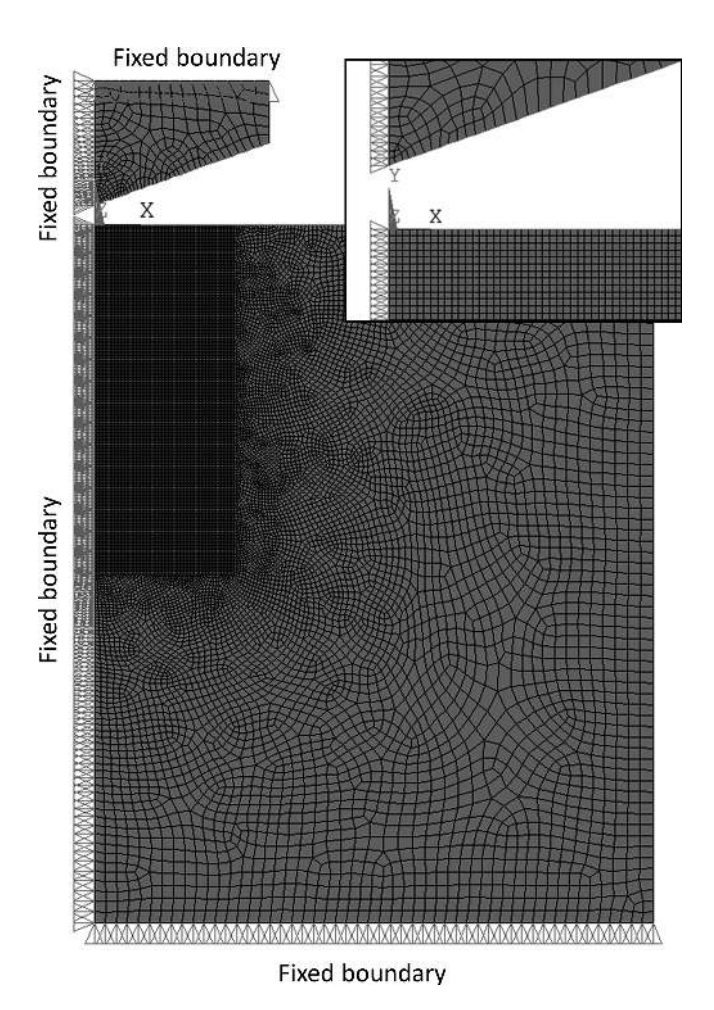


Fig. 1. Finite element model mesh for indenter and substrate showing smaller mesh size in the contact area.

Table 1. The input and expected values of mechanical properties for the finite element simulations of the different materials.

Model input & mechanical	Nominal material type						
property	Fused Silica	Aluminum Alloy 8009	Aluminum	Iron	ZnO	Sapphire	
Elastic Modulus, E (GPa)	72	82.1	70	210	149	458	
Poisson's Ratio, v	0.18	0.31	0.3	0.3	0.2	0.2	
Reduced Modulus, $E_{\rm r}$ (GPa)	69.9	84.2	72.1	192.1	136.7	336.9	
Yield Stress (GPa)	2.5	0.353	0.083	0.325	2.267	15.33	
Tangent Modulus, $E_{\rm t}$ (GPa)	17.38	_	1.032	5.8	_	_	
Hardness, H (GPa)	9.3	1.2	0.48	1.2	4.8	25	
Maximum Indenter Displacement (nm)	2075	1750	2 200	178	1870	1 000	
Ratio of <i>H/E</i>	0.1292	0.0146	0.0069	0.0057	0.0322	0.0546	
Ratio of <i>H/E</i> _r	0.133	0.0143	0.0067	0.0062	0.0351	0.0742	

approach similar to the unloading curve analysis to find the reduced elastic modulus enables the hardness to be found from Eqs. (2) and (11) without using Eq. (3).

Examining a number of different materials with known properties and performing a least squares fit to the resulting data it is possible to find the parameter Π_{θ} in Eq. (11). Once Π_{θ} is known the method can be used to analyze load–depth curves to quantify mechanical properties. This requires the work of loading and unloading to be found from the different parts of a load–depth curve by numerically integrating to find the area under the curves. Eq. (11) is then used to relate these to the mechanical properties.

3. Finite element simulation and analysis procedure

The nanoindentation process was simulated using the axisymmetric features of the ANSYSTM finite element software package. Realistic stress-strain curves were used to capture the elastic and plastic behaviors of materials with a range of different properties. The indenter tip was modeled as a cone with the angle set equal to 70.3° to ensure the cross-sectional area of the cone is equivalent to that of an ideal Berkovich pyramid. The indentation depths and dimensions of the specimens modeled using FEM varied from one material to another, but in many cases the materials and the depths were chosen to replicate published results [1, 28, 29, 31, 35]. A typical finite element mesh and the boundary conditions applied are shown in Fig. 1. A very fine mesh was deployed in the contact region to adequately resolve the large stress and strain gradients that are present during the nanoindentation procedure. This also allowed accurate determination of the contact area directly from the simulations. With reference to Fig. 1, it can be seen that symmetry boundary conditions were imposed along the yaxis (along the center of the conical indenter). Additionally, the specimen was simply supported, and the indentation was made via an imposed displacement at the upper surface of the indenter. Friction between the indenter and the material's surface was assumed to be zero. Note that due to the axisymmetric nature of the model the specific geometry of the substrate was a flat-ended cylinder, while the indenter was a conical-tipped cylinder. For all analyzes the specimen dimensions were chosen to be sufficiently large as to approximate the behavior of a semi-infinite half-space. This was ensured by increasing the specimen dimensions to the point where the results became insensitive to size.

A wide range of mechanical properties (see Table 1) with various nonlinear stress–strain curves were used to replicate different materials during the FEM nanoindentation simulations. Table 1 details the elastic modulus, Poisson's ratio, yield stress, and tangent modulus (where applicable) that were used for a given simulation. Additionally, the table includes the maximum indentation depth used for each simulation and the literature value of hardness for the material being replicated [1, 28, 29, 31, 35]. To model the nonlinear yield behavior either bilinear or multi–linear isotropic hardening models were used to replicate the stress–strain curves of the materials. Plots of these stress–strain curves are presented in Fig. 2.

ANSYSTM Parametric Design Language (APDL) files were created to facilitate simulations and to improve data extraction efficiencies. Finite element simulations produce significant amounts of output so a level of automation is es-

sential for data extraction and supplemental calculations. The ANSYSTM output included information such as: (1) indenter forces, displacements, stresses, and strains; (2) specimen deformations, stresses, and strains. The specimen stresses and strains consisted of both elastic and plastic components. Thus, upon simulated retraction of the inden-

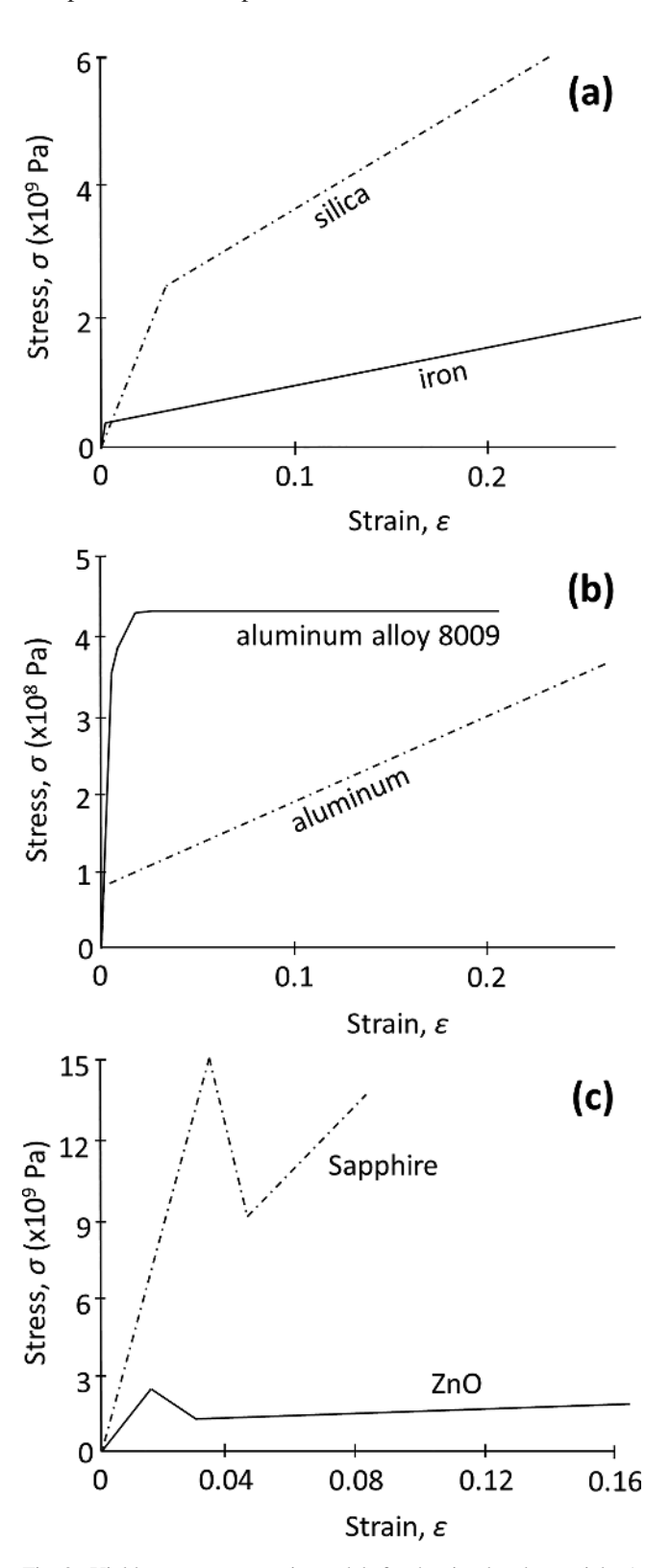


Fig. 2. Yield stress versus strain models for the simulated materials. A range of yield behaviors were modeled with different assumptions for strain hardening.

ter, residual stresses and strains were observed in the specimens, along with permanent deformations due to plasticity. Using the indenter forces and displacements provided by the finite element simulations of each of the materials (given in Table 1) curves of load versus depth were created for the loading and unloading segments of the nanoindentation cycle.

The predicted loading and unloading curves were used as the basis for comparing the three methods of analysis previously discussed. To implement the unloading curve analysis, the FEM load-depth data for the unloading curves were fitted to Eq. (1) using MATLABTM. The mechanical properties were then found using Eqs. (2), (3), (4) and (5). For the loading curve analysis the FEM load-depth data for the loading curve was fitted to an equation of the form Eq. (9) for each of the materials modeled. Subsequently, the values of Φ and ψ consistent with optimizing Eq. (10) were found from the fits of the loading curve for all the materials. Lastly, for the work of indentation analysis the integrated area under the loading and unloading curves were used to find the total work and elastic work of indentation, respectively, for each material. As with the other curve fitting procedures, MATLABTM was used and a curve fit to Eq. (11) was performed to find the value of the parameter Π_{θ} that relates hardness, elastic modulus, and work. The value of Π_{θ} was optimized across all the materials. Once Π_{θ} was found the Cheng & Cheng [3] method was implemented to find H/E_r for each material from the loading and unloading curves with the aid of Eq. (11).

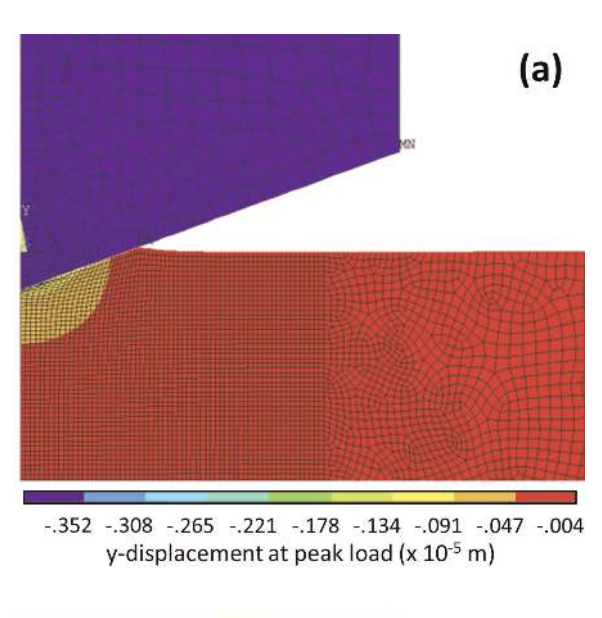
4. Results and discussion

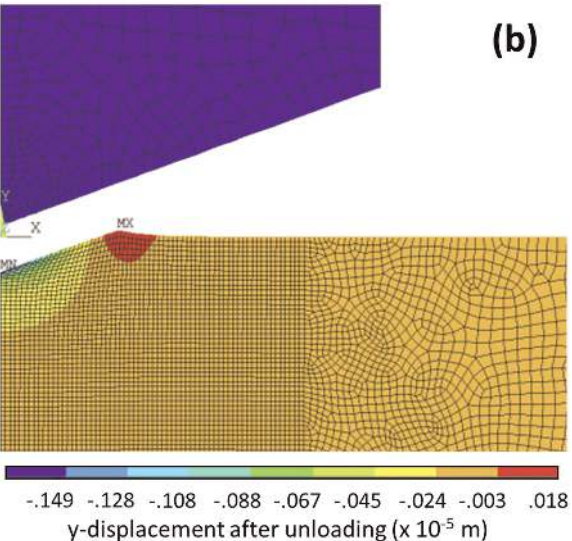
Numerous FEM simulations were needed to compare the different analysis methods. As previously mentioned, several different sets of material properties were considered for this purpose and they were chosen to have similar properties to fused silica, aluminum alloy 8009, pure aluminum, iron, ZnO, and sapphire.

Figure 3 shows contour plots generated by the finite element software when simulating indentation for a soft, ductile material which in this particular case is replicating aluminum alloy 8009. These contour plots show many of the key features seen for the other materials, though not all of them are shown here for brevity. The vertical displacement (*y*-component) of the material (replicating aluminum alloy 8009) under peak loading is shown by Fig. 3a. This plot shows the indenter at its maximum displacement of 1750 nm, though the maximum deformation of the specimen is 1732.9 nm. The variance between these two values is due to the compliance of the simulated diamond indenter. It should be noted that this variance is exacerbated when simulating materials with elastic moduli approaching that of diamond; in this study that is sapphire.

The surface deformation for the simulated aluminum alloy 8009 after the indenter has been removed is illustrated in Fig. 3b. In this case the maximum residual displacement $h_{\rm m}$ in the substrate is 1594 nm. For this material, and for the other ductile materials simulated, pile-up is evident at the edges of the indent. Figure 3c shows the residual stress field in the y-direction, σ_y , that persists in the specimen after the indenter's removal.

Load-depth curves for all of the FEM simulations are presented in Fig. 4a to f with the depth being the displace-





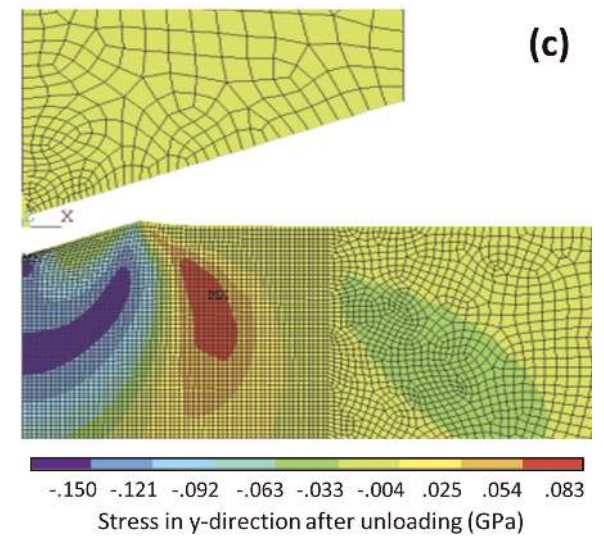


Fig. 3. The results of the simulations for one material, aluminum alloy 8009. (a) Maximum vertical displacement of indenter into the material showing the extent of the deformation; (b) Permanent vertical deformation after the removal of the indenter with the indenter impression in the surface and pile-up at the indent edge; (c) Residual stress, σ , in y-direction after unloading.

ment of the indenter without correction for the indenter compliance. The maximum specimen displacements (including the correction for the indenter compliance) are also shown in these figures. For several of the curves, each specimen material is relatively compliant compared to the diamond indenter, hence the specimen and indenter curves essentially overlap one another. For simulations replicating pure aluminum (Fig. 4b) at the maximum applied indenter displacement of 2 200 nm, the maximum vertical displacement of the specimen is 2 185.3 nm. An indenter force of 64 mN was required to produce this deformation. Note that a permanent deformation of 2 107 nm remains for this par-

ticular simulation even after the indenter has been retracted.

When the stiffness of a specimen approaches that of the indenter, the compliance of the indenter leads to larger variances between the applied indenter depth and the specimen's maximum deformation. This effect is acutely apparent in Fig. 4f where the simulation involves sapphire, which has an elastic modulus approximately 40% of the diamond indenter's elastic modulus. During the FEM simulated nanoindentation, an applied indenter depth of 500 nm produces a maximum specimen deformation of only 437.9 nm due to compression in the diamond indenter.

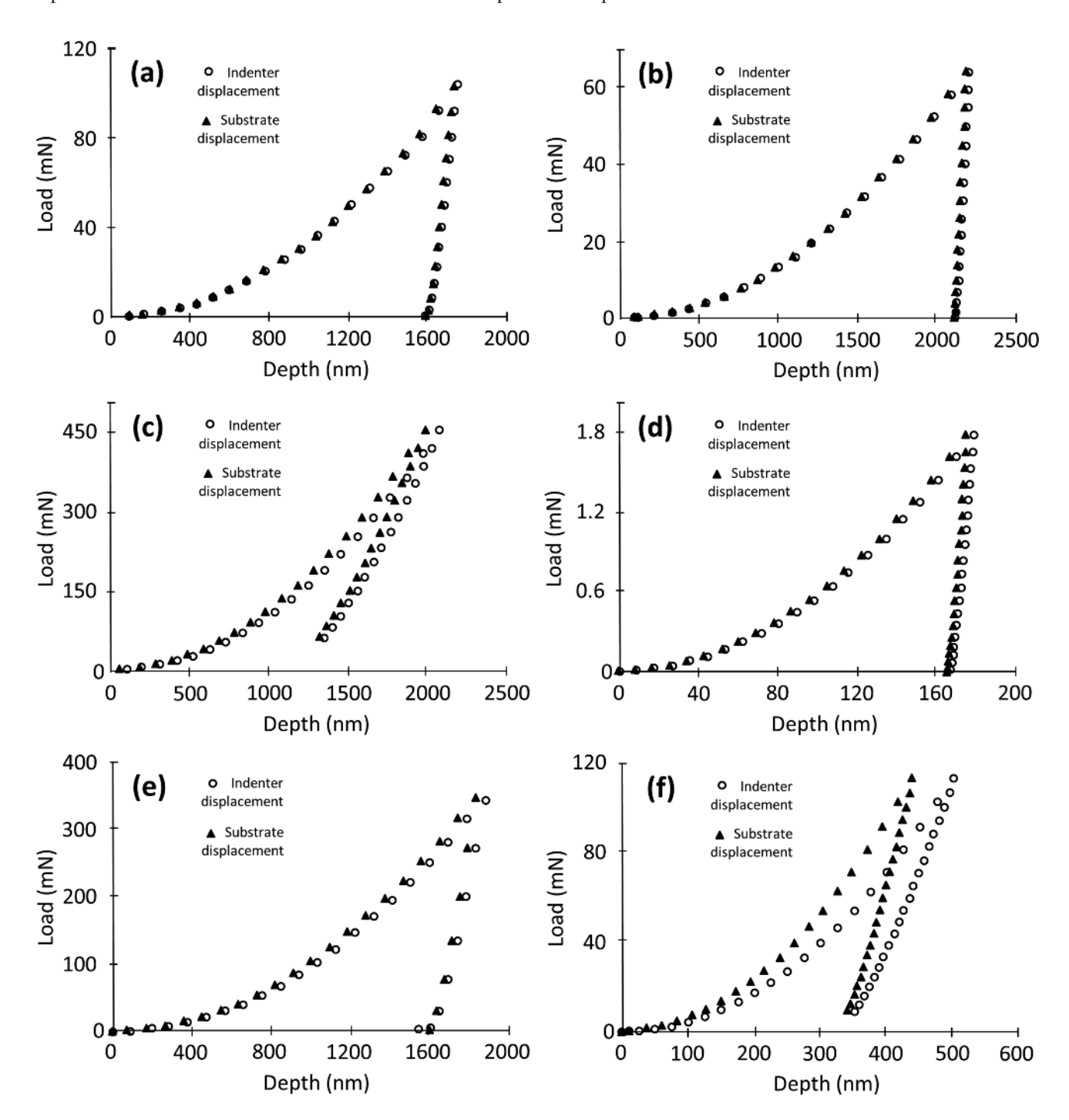


Fig. 4. Load–depth curves obtained from finite element simulations showing both the indenter and substrate displacements for (a) 8009 aluminum, (b) aluminum, (c) fused silica, (d) iron, (e) ZnO, and (f) sapphire. The materials with higher mechanical properties cause significant deformation of the indenter and, hence, there is a difference between the indenter and substrate displacements.

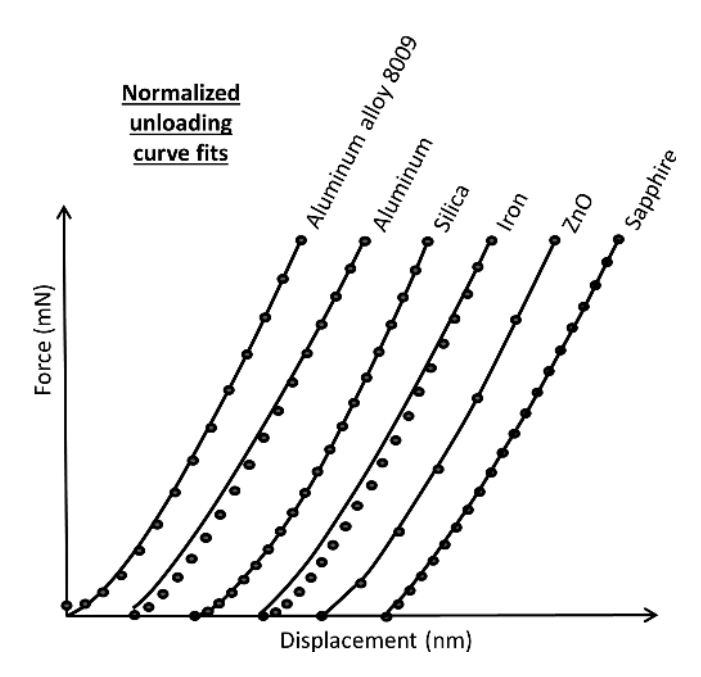


Fig. 5. Unloading curve fits for each of the simulated materials based on Eq. (1). Note the origins of the curves are displaced to fit them all on the same plot.

4.1. Unloading curve analysis

The standard unloading curve analysis based on Eq. (1) was fitted to all of the FEM simulations, as illustrated in Fig. 5. The figure shows that the fitting procedure generally yielded good results, along with excellent fits in some cases. With respect to the FEM results the exponent curve fit parameter m in Eq. (1) spanned a relatively narrow band from 1.2681 (aluminum alloy 8009) to 1.4869 (fused silica). The other fitting parameter, β in Eq. (1), is most easily found in terms of its reciprocal $1/\beta$ which ranged from 0.0159 for fused silica to 0.205 for ZnO. Using these curve fit parameters, the contact stiffness for each of the simulated nanoindentation experiments was obtained. In addition, Eqs. (5) and (6) were used, respectively, to calculate the contact depth and the projected contact area corresponding to the maximum indenter load. The hardness and elastic modulus properties were evaluated using Eqs. (2) and (3). Importantly this method when compared to published and expected values for the elastic modulus and hardness yielded predictions that were sometimes very accurate and generally good. Table 2 lists each of the simulated materials along with the material property predictions obtained using the standard (Oliver & Pharr [1]) method.

The accuracy of the elastic modulus and hardness obtained by analyzing the FEM unloading curves was compared to the input values. For elastic modulus, which was expected to be closest to the input values, the errors ranged from a low of less than 1.9% to a high of about 26.5% (this was an outlier since the average error was only 11%). The hardness predictions were found to have a higher average error of about 29%, though there is a higher-level of uncertainly in the published hardness data so these discrepancies are somewhat expected. In Table 2, we see that the relative errors in hardness range from a low of 0.7% for ZnO to a high of almost 105% for iron. The hardness prediction for iron appears to be an aberration when the average hardness

error is taken into consideration. Overall, of the methods of analysis considered the unloading curve method based on the work of Oliver & Pharr [1, 22] produced the most consistent match with the published and expected values for elastic modulus and hardness.

4.2. Loading curve analysis

The loading curve analysis provides the ratio of hardness to elastic modulus (H/E). The loading curve data generated by the FEM simulations along with the parabolic curve fits required for the analysis, are shown in Fig. 6. The figure shows the excellent fit between the FEM load curves and the parabolic functions indicating that the assumption of a parabolic loading curve shape is valid. The parabolic curve fit coefficient, $K_{\rm m}$ in Eq. (8), for each of the FEM simulations ranges from 13.26 for aluminum to 445.68 for sapphire in units of GPa. Using Eq. (10), it was determined that the optimal values for the fitting parameters Φ and ψ were, respectively, 0.1970 and 0.7548. As depicted in Fig. 7, the quality of the curve fit incorporating these optimal values is good. The plot shows the values of $K_{\rm m}$ obtained from the individual load-depth curves versus those obtained using the fitting parameters $\Phi = 0.1970$ and $\psi = 0.7548$.

Comparing the expected values of H/E to the values given by the loading analysis (see Table 2) it can be seen that there is a very good match for some of the simulated materials, notably sapphire and ZnO. The other data are not such a good match with the worst being the value for iron which is off by over 100%. Combining this method with the approach deployed in the unloading curve analysis of Oliver & Pharr [1, 22] enables either elastic modulus or hardness to be found using the loading fit. As would be expected this gave good values of H and E for the simulated sapphire and aluminum, and very poor values for iron. The other simulated materials were between these extremes.

4.3. Work of indentation analysis

Application of the area under the curves or work of indentation method produced results that were comparable in accuracy to those obtained when utilizing the unloading curve method. The work of indentation analysis gives the ratio of hardness to reduced elastic modulus (H/E_r) using Eq. (11). The fitting parameter Π_{θ} used in Eq. (11) was found from a best fit to all the simulated materials. This gave a value of $\Pi_{\theta} = 0.1413$ as the best fit which is represented by the solid line on the plot for all the materials given in Fig. 8. Using Eq. (11) the material properties were calculated and these are presented in Table 2 where they are compared to their respective expected values. As seen in this table, the results are generally good for H/E_r , with the simulated sapphire, aluminum and aluminum 8009 alloy all close to their expected values. Analysis of the simulated ZnO, fused silica and iron curves showed the method was somewhat inaccurate in terms of H/E_r , with iron being the most inaccurate.

Combining the work of indentation analysis with the equations used in the unloading analysis it was possible to find either the elastic modulus or the hardness for each of the simulated materials. This gave elastic modulus values with errors that were comparable to (or even slightly better) than those obtained from the unloading curve analysis on its own.

5. Conclusions

The standard unloading curve method [1, 22], the loading curve method [2, 33] and the work of indentation [3, 34] have been used to analyze loading and unloading curves produced using FEM for materials with a wide range of properties. Fits to the FEM load–depth curves for each of the methods are very good indicating the basic assumptions with regards to curve shape are valid for each of the methods. That is, Eq. (1) for the unloading analysis fits the unloading curve well, the parabolic loading curve implied by Eq. (8) is an excellent fit to the FEM loading curves, and the work of indentation analysis using Eq. (11) gives a close fit to the observed areas under the load–depth curves.

Extracting the hardness, elastic modulus and their ratios from the fits determines the overall accuracy of the methods. In this regard the maturity of the unloading curve analysis, which in various forms has been used for over 30 years, gives it an advantage with the properties having values consistently close to those expected. This is also a

reflection of the general robustness of the method for analyzing data from a variety of materials. The unloading curve analysis provides a direct way to find the values for elastic modulus and hardness rather than a ratio of the two as obtained with the other methods. Very good property predictions are obtained from the work of indentation method for most of the materials modeled, though there were large discrepancies in some cases. When comparing the best results from the unloading curve analysis to the best from a combination of the unloading analysis and work of indentation it was found that the combination gave slightly more accurate values. These two methods make similar assumptions in the analysis and, hence, it is not surprising that they are comparable in accuracy and can be combined to give slightly better results.

Analysis of the loading curve fit was found to give the least accurate values for the properties despite the fact that the parabolic curve fits were remarkably good (see Fig. 6). However, it should be noted that other researchers have found good fits to the loading curve using functions that

Table 2. Comparison of the results for the unloading curve, loading curve and indentation work analysis. The values in parentheses are the percentage difference compared to the expected values (Table 1).

	Fused Silica	Aluminum Alloy 8009	Aluminum	Iron	ZnO	Sapphire
Unloading,	7.3	1.5	0.5	2.5	4.8	28
H (GPa)	(-21.5%)	(25.0%)	(4.2 %)	(108.3 %)	(0.0%)	(12.0%)
Unloading, $E_{\rm r}$ (GPa)	76.2	89.9	73.4	185.6	167.6	374.6
	(9.0%)	(6.8 %)	(1.8 %)	(-3.4%)	(22.6%)	(11.2%)
Unloading,	79	88.1	71.3	201.5	188.5	534.1
E (GPa)	(9.7 <i>%</i>)	(7.3 %)	(1.9%)	(-4.0%)	(26.5%)	(16.6%)
Unloading,	0.0924	0.0170	0.0070	0.0124	0.0255	0.0524
<i>H/E</i>	(-28.5 %)	(16.6%)	(1.6%)	(118%)	(-20.9%)	(-4.0%)
Unloading, $H/E_{\rm r}$	0.0958	0.0167	0.0068	0.0135	0.0286	0.0747
	(-28.0%)	(16.7%)	(1.5 %)	(117.7%)	(-18.4%)	(0.7%)
Loading,	7.3	1.5	0.5	2.5	4.8	28
(GPa)	(-21.5 %)	(25.0%)	(4.2 %)	(108.3 %)	(0.0%)	(12.0%)
Loading, $E_{\rm r}$ (GPa)	79.1	71	206.2	134.5	144.9	302.1
	(13.2%)	(-15.7 %)	(186.0%)	(-30.0%)	(6.0%)	(-10.3 %)
Loading,	82.2	68.4	228.8	138.7	159.2	393.7
E (GPa)	(14.2 <i>%</i>)	(-16.7 %)	(226.9%)	(-34.0%)	(6.8%)	(-14.0%)
Loading,	0.0888	0.0219	0.0022	0.0180	0.0302	0.0711
H/E	(-31.3%)	(50.2%)	(-68.3%)	(216.2%)	(-6.36%)	(30.3 %)
Loading, $H/E_{\rm r}$	0.0923	0.0211	0.0024	0.0186	0.0331	0.0927
	(-30.6%)	(47.7%)	(-64.2%)	(199.8 %)	(-5.62%)	(24.9 %)
Indent work,	6.3	1.5	0.5	2.3	4.6	28.6
H (GPa)	(-32.3 %)	(25.0%)	(4.2 %)	(91.7 %)	(-4.2%)	(14.4%)
Indent work, $E_{\rm r}$ (GPa)	76.2	89.9	73.4	185.6	167.6	374.6
	(9.0%)	(6.8 %)	(1.8 %)	(-3.4%)	(22.6%)	(11.2 <i>%</i>)
Indent work,	73.8	81.2	66.8	168.9	160.9	359.6
E (GPa)	(2.5 %)	(-1.1%)	(-4.6%)	(-19.6 %)	(8 %)	(-21.5 %)
Indent work, <i>H/E</i>	0.0854	0.0185	0.0075	0.0136	0.0286	0.0795
	(-33.9%)	(26.5%)	(8.5 %)	(138.9%)	(-11.2%)	(45.7 %)
Indent work, H/E _r	0.0827	0.0167	0.0068	0.0124	0.0274	0.0763
	(-37.8%)	(16.7%)	(1.5 %)	(99.9%)	(-21.8%)	(2.9%)

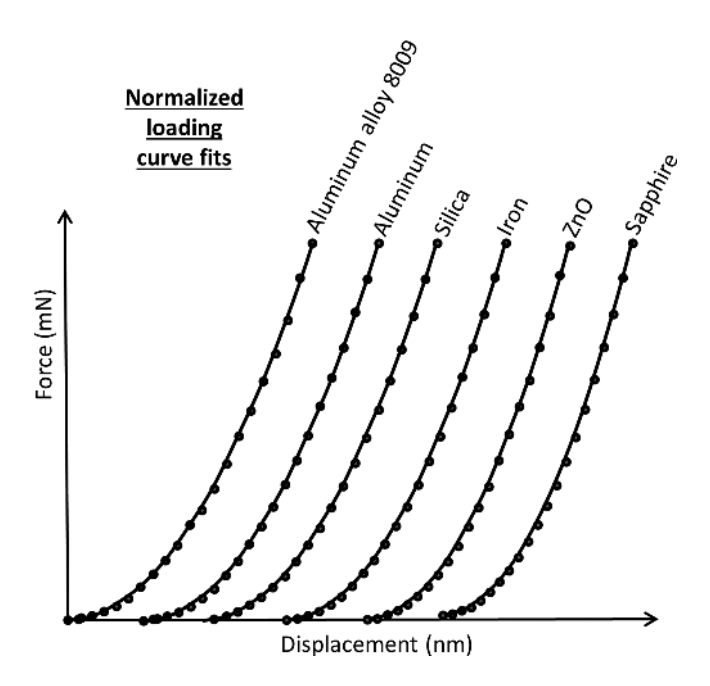


Fig. 6. Parabolic loading curve fits for each of the simulated materials based on Eq. (8). Note the origins of the curves are displaced to fit them all on the same plot.

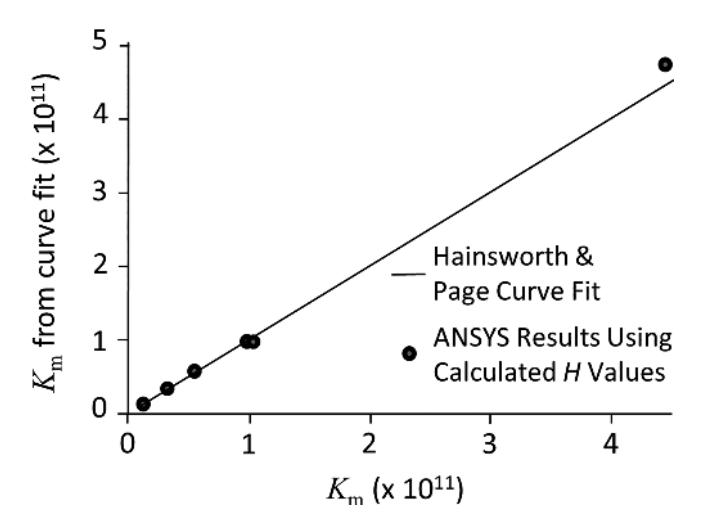


Fig. 7. Plot of the parabolic loading curve fitting value, K_m in Eq. (9). The value of individual load–depth curves for each sample are the data points. The line is the value expected using the best fit parameters $\Phi = 0.1970$ and $\psi = 0.7548$.

are not parabolic [13]. With the loading curve method, the predicted values for the materials exhibiting significant work-hardening, aluminum and iron, were very poor suggesting that the assumption of a constant *E/H* ratio in Eq. (9) is an issue. Given the quality of the curve fit, there appears to be scope to develop this analysis further, in particular as a complementary method to the unloading curve analysis.

A well-known issue with load—depth curve analysis is the effect of pile-up or sink-in at the edge of the contact affecting the contact geometry and, hence, contact area. This change in contact geometry depends on several factors including: the ratio of yield stress to elasticity for a material (which is related to *H/E*); the extent of work hardening; the presence of residual stresses at the surface. In general,

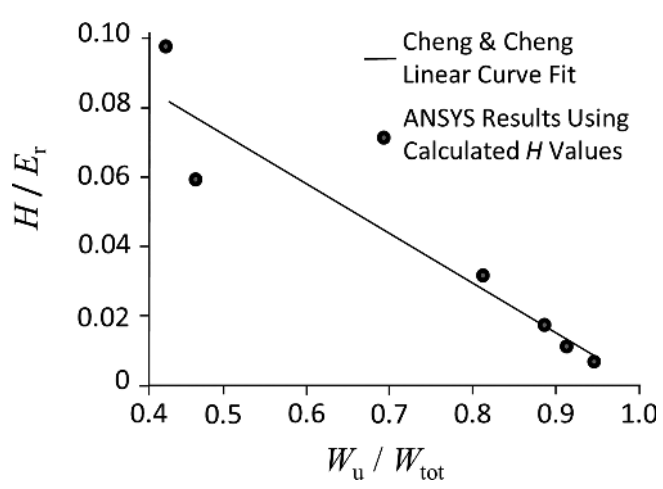


Fig. 8. Ratio of hardness to reduced modulus as a function of the work of indentation (ratio of unloading work to total work). The individual points for each sample (data points) and the best fit for Eq. (11) are shown

compressive stress and low H/E favors pile-up, while tensile stress and high H/E favors sink-in. These geometry changes impact all of the analysis methods, but the unloading curve analysis explicitly uses contact area to find $E_{\rm r}$ and H so it is very susceptible to errors in contact geometry. The loading curve and work of indentation methods are better in this regard as they do not use contact area to find the ratios of H/E or $H/E_{\rm r}$. It is interesting to note that across all of the analysis methods the least accurate values were obtained for the simulated iron and aluminum. In both cases the hardness relative to elastic modulus is very low, and there is linear strain-hardening. For the unloading analysis, pile-up gives significant contact area errors, while for the other two methods the strain-hardening results in changes in hardness with depth.

Fitting of the FEM load-depth curves shows that all of the methods of analysis give significant discrepancies from the expected values for some of the materials simulated, though each method also gives very good results for some of the simulated curves. Going forward, it is likely that the best results for analyzing real curves may come from unifying the different methods into a single methodology. This is likely to require refinements of the loading curve analysis to ensure compatibility with the other methods. A single, integrated analysis methodology could offer a way to overcome the specific weaknesses of the individual analysis routines.

This material is based in part upon work supported by the National Science Foundation under Grant No. 1006723.

References

- [1] W.C. Oliver, G.M. Pharr: J. Mater. Res. 7 (1992) 1564. DOI:10.1557/JMR.1992.1564
- [2] S.V. Hainsworth, H.W. Chandler, T.F. Page: J. Mater. Res. 11 (1996) 1987. DOI:10.1557/JMR.1996.0250
- [3] Y.T. Cheng, C.M. Cheng: Appl. Phys. Lett. 73 (1998) 614. DOI:10.1063/1.121873
- [4] R. Saha, W.D. Nix: Acta Mater. 50 (2002) 23. DOI:10.1016/S1359-6454(01)00328-7
- [5] W.J. Poole, M.F. Ashby, N.A. Fleck: Scr. Mater. 34 (1996) 559.DOI:10.1016/1359-6462(95)00524-2
- [6] C.A. Schuh: Mater. Today 9 (2006) 32. DOI:10.1016/S1369-7021(06)71495-X

- [7] S.R. Kalidindi, S.J. Vachhani: Curr. Opin. Solid State Mater. Sci. 18 (2014) 196. DOI:10.1016/j.cossms.2014.05.002
- [8] G. Alcala, S. Mato, P. Skeldon, G.E. Thompson, A.B. Mann, H. Habazaki, K. Shimizu: Surf. Coat. Technol. 173 (2003) 293– 298. DOI:10.1016/S0257-8972(03)00738-2
- [9] N. Chollacoop, M. Dao, S. Suresh: Acta Mater. 51 (2003) 3713. DOI:10.1016/S1359-6454(03)00186-1
- [10] N. Raykar, V. Gupta, B. Kear, M. Chhowalla, A.B. Mann: Scr. Mater. 57 (2007) 925. DOI:10.1016/j.scriptamat.2007.07.022
- [11] J. Malzbender, G. de With, J. den Toonder: J. Mater. Res. 15 (2000) 1209. DOI:10.1557/JMR.2000.0171
- [12] C.L. Hu, Z.J. Li: Constr. Build. Mater. 90 (2015) 80. DOI:10.1016/j.conbuildmat.2015.05.008
- [13] S.J. Bull: J. Phys. D Appl. Phys. 38 (2005) R393. DOI:10.1088/0022-3727/38/24/R01
- [14] J. Chen, S.J. Bull: Int. J. Mater. Res. 99 (2008) 852. DOI:10.3139/146.101709
- [15] M.R. Naimi-Jamal, G. Kaupp: Z. Metallkd. 96 (2005) 1226– 1236. DOI:10.3139/146.101166
- [16] C.E. Beck, F. Hofmann, J.K. Eliason, A.A. Maznev, K.A. Nelson, D.E.J. Armstrong: Scr. Mater. 128 (2017) 83. DOI:10.1016/j.scriptamat.2016.09.037
- [17] T. Andriollo, J. Thorborg, J. Hattel: Model. Simul. Mater. Sci. Eng. 25 (2017) Article Number: 045004. DOI:10.1088/1361-651X/aa6831
- [18] J.L. Loubet, J.M. Georges, J.M. Marchesini, G. Meille: J. Tribol.-T ASME 106 (1984) 43. DOI:10.1115/1.3260865
- [19] J.L. Loubet, J.M. Georges, G. Meille, in: P.J. Blau, B.R. Lawn (Eds.), Microindentation Techniques in Materials Science and Engineering, ASTM International (1985) 72. DOI:10.1520/STP32952S
- [20] M.F. Doerner, W.D. Nix: J. Mater. Res. 1 (1986) 601. DOI:10.1557/JMR.1986.0601
- [21] S.I. Bulychev, V.P. Alekhin, M.Kh. Shorshorov, A.P. Ternovskij, G.D. Shnyrev: Ind. Lab-USSR+ 41 (1975) 1137.
- [22] W.C. Oliver, G.M. Pharr: J. Mater. Res. 19 (2004) 3. DOI:10.1557/jmr.2004.0002
- [23] I.N. Sneddon: Int. J. Eng. Sci. 3 (1965) 47. DOI:10.1016/0020-7225(65)90019-4
- [24] J.W. Harding, I.N. Sneddon: Math. Proc. Cambridge. 41 (1945) 16. DOI:10.1017/S0305004100022325
- [25] G.M. Pharr, W.C. Oliver, F.R. Brotzen: J. Mater. Res. 7 (1992) 613. DOI:10.1557/JMR.1992.0613
- [26] J.A. Knapp, D.M. Follstaedt, S.M. Myers, J.C. Barbour, T.A. Friedmann: J. Appl. Phys. 85 (1999) 1460. DOI:10.1063/1.369178
- [27] A. Bolshakov, G.M. Pharr: J. Mater. Res. 13 (1998) 1049.

- DOI:10.1557/JMR.1998.0146
- [28] T.Y. Tsui, W.C. Oliver, G.M. Pharr: J. Mater. Res. 11 (1996) 752. DOI:10.1557/JMR.1996.0091
- [29] A. Bolshakov, W.C. Oliver, G.M. Pharr: J. Mater. Res. 11 (1996) 760. DOI:10.1557/JMR.1996.0092
- [30] J.C. Hay, A. Bolshakov, G.M. Pharr: J. Mater. Res. 14 (1999) 2296–2305. DOI:10.1557/JMR.1999.0306
- [31] G.M. Pharr, A. Bolshakov: J. Mater. Res. 17 (2002) 2660. DOI:10.1557/JMR.2002.0386
- [32] N. Yu, A.A. Polycarpou, T.F. Conry: Thin Solid Films 450 (2004) 295. DOI:10.1016/j.tsf.2003.10.033
- [33] S.V. Hainsworth, M.R. McGurk, T.F. Page: Surf. Coat. Technol. 102 (1998) 97. DOI:10.1016/S0257-8972(97)00683-X
- [34] Y.T. Cheng, C.M. Cheng: Surf. Coat. Technol. 133 (2000) 417. DOI:10.1016/S0257-8972(00)00896-3
- [35] S. Basu, A. Moseson, M.W. Barsoum: J. Mater. Res. 21 (2006) 2628. DOI:10.1557/JMR.2006.0324

(Received May 31, 2018; accepted July 30, 2018; online since November 5, 2018)

Correspondence address

Adrian B. Mann Materials Science & Engineering Department Rutgers University 607 Taylor Road Piscataway NJ 08854 USA

Tel.: +18484458421

E-mail: abmann@soe.rutgers.edu

Web: http://www.rci.rutgers.edu/~abmann/

Bibliography

DOI 10.3139/146.111720

Int. J. Mater. Res. (formerly Z. Metallkd.) 110 (2019) 2; page 91–100

© Carl Hanser Verlag GmbH & Co. KG ISSN 1862-5282